THE JOURNAL OF BIOLOGICAL CHEMISTRY VOL. 286, NO. 24, pp. 21266–21276, June 17, 2011

Studies on Lactoferricin-derived *Escherichia coli* Membrane-active Peptides Reveal Differences in the Mechanism of *N*-Acylated *Versus* Nonacylated Peptides*

Received for publication, October 18, 2010, and in revised form, April 5, 2011 Published, JBC Papers in Press, April 22, 2011, DOI 10.1074/jbc.M110.195412

Dagmar Zweytick[‡], Günter Deutsch[‡], Jörg Andrä[§1], Sylvie E. Blondelle[¶2], Ekkehard Vollmer[‖], Roman Jerala[3], and Karl Lohner[‡4]**

*From the [‡]Institute of Biophysics and Nanosystems Research, Austrian Academy of Sciences, Schmiedlstrasse 6, A-8042 Graz, Austria, the [§]Division of Biophysics, Research Center Borstel, Leibniz-Center for Medicine and Biosciences, Parkallee 10, D-23845 Borstel, Germany, the [¶]Torrey Pines Institute for Molecular Studies, San Diego, California 92121, the [‖]Division of Clinical and Experimental Pathology, Research Center Borstel, Leibniz-Center for Medicine and Biosciences, Parkallee 3a, D-23845 Borstel, Germany, and the **Department of Biotechnology, National Institute of Chemistry, the EN-FIST Centre of Excellence, and the Faculty of Chemistry and Chemical Technology, University of Ljubljana, Hajdrihova 19, SI-1000 Ljubljana, Slovenia*

To improve the low antimicrobial activity of LF11, an 11-mer peptide derived from human lactoferricin, mutant sequences were designed based on the defined structure of LF11 in the lipidic environment. Thus, deletion of noncharged polar residues and strengthening of the hydrophobic N-terminal part upon adding a bulky hydrophobic amino acid or *N*-acylation resulted in enhanced antimicrobial activity against *Escherichia coli*, which correlated with the peptides' degree of perturbation of bacterial membrane mimics. Nonacylated and *N*-acylated peptides exhibited different effects at a molecular level. Nonacylated peptides induced segregation of peptide-enriched and peptide-poor lipid domains in negatively charged bilayers, although *N*-acylated peptides formed small heterogeneous domains resulting in a higher degree of packing defects. Additionally, only *N*-acylated peptides perturbed the lateral packing of neutral lipids and exhibited increased permeability of *E. coli* lipid vesicles. The latter did not correlate with the extent of improvement of the antimicrobial activity, which could be explained by the fact that elevated binding of *N*-acylated peptides to lipopolysaccharides of the outer membrane of Gram-negative bacteria seems to counteract the elevated membrane permeabilization, reflected in the respective minimal inhibitory concentration for *E. coli*. The antimicrobial activity of the peptides correlated with an increase of membrane curvature stress and hence bilayer instability. Transmission electron microscopy revealed that only the *N*-acylated peptides induced tubular protrusions from the outer membrane, whereas all peptides caused detachment of the outer and inner membrane of *E. coli* bacteria. Viability tests demonstrated that these bacteria were dead before onset of visible cell lysis.

Lactoferrin (LF)[5] is an iron-binding glycoprotein found in milk (1) and in exocrine secretions of mammals as well as in granules and neutrophils during inflammatory responses (2, 3). The pepsin cleavage fragment lactoferricin, comprising amino acid residues 1–45 of the N terminus of human LF and 17–41 of bovine LF, is one example of naturally occurring antimicrobial peptides (4). Lactoferricin displays activity against a diverse range of microorganisms such as Gram-negative bacteria, Gram-positive bacteria, yeast, and filamentous fungi, including a number of antibiotic-resistant pathogens (4). It is assumed that lactoferricin permeabilizes cell membranes and exerts anti-endotoxic activity by binding to lipopolysaccharides (4). In earlier studies, we demonstrated that the stretch of 11 amino acid residues (LF11, FQWQRNIRKVR-NH_2) corresponding to LF residues 21–31 exhibits only weak antibacterial activity against a number of Gram-positive and Gram-negative bacterial strains (5, 6). A series of about 150 LF11 mutants was designed with the aim to strengthen membrane-peptide interactions and hence to generate highly antimicrobial and endotoxin-neutralizing peptides, while having no or little antigenic or toxic effect on humans. Our strategy was based on the premise that positive net charge and hydrophobicity are fundamental factors for antimicrobial activity, the former governing affinity for negatively charged membranes and the latter membrane insertion of the peptides and thus membrane damage (7, 8). Single or multiple point mutations in LF11 lead to peptide derivatives having up to 30-fold increase in antimicrobial activity (9, 10). Another approach was to increase the hydrophobicity by adding a hydrophobic moiety to the peptide (6). For example, Wakabayashi *et al.* (4, 11) and Strom *et al.* (12) have shown that *N*-acylation of derivatives based on a sequence of bovine lactoferricin B (amino acids 17–41) resulted in higher

* This work was supported in part by EC-specific RTD Programme Grant QLK2-CT-2002-01001, "Antimicrobial Endotoxin Neutralizing Peptides to Combat Infectious Diseases."
[1] Supported by German Science Foundation Grant AN301/5-1.
[2] Present address: Sanford-Burnham Medical Research Institute, 10901 North Torrey Pines Rd., La Jolla, CA 92037.
[3] Supported by the Slovenian Research Agency and EN-FIST Centre of Excellence.
[4] To whom correspondence should be addressed. Tel.: 43-316-4120-323; Fax: 43-316-4120-390; E-mail: karl.lohner@oeaw.ac.at.

[5] The abbreviations used are: LF, lactoferrin; POPE, 1-palmitoyl-2-oleoyl-*sn*-glycero-3-phosphoethanolamine; DPPG, 1,2-dipalmitoylphosphatidylglycerol; PE, phosphatidylethanolamine; ANTS, 8-aminonaphthalene-1,3,6-trisulfonic acid; DPX, *p*-xylene-bis-pyridinium bromide; MNC, mononuclear cell; LUV, large unilamellar vesicle; DSC, differential scanning calorimetry; TEM, transmission electron microscopy; SAXS, small angle x-ray scattering; 6-MO, 6-methyloctanoyl; MIC, minimal inhibitory concentration.

antimicrobial activity. Nevertheless, an increase in hydrophobicity above a certain threshold value can also result in a loss of membrane specificity, *i.e.* damage of mammalian cells, as we observed for the *N*-lauryl derivative of LF11, which exhibited diminished selectivity (6). To further investigate the effect of peptide *N*-acylation on peptide specificity, different acyl groups were attached to the N terminus of LF11 peptides to increase their specificity toward bacterial *versus* mammalian cells (6, 13, 14, 44). The biophysical studies revealed a chain length-dependent membrane perturbation in agreement with biological activity data with an optimum chain length of eight carbon atoms. For example, 6-methyloctanoyl as a hydrophobic group, which mimics the potent antimicrobial peptide polymyxin B (15), strongly improved the activity against *Escherichia coli*. Therefore, this study focuses on the effect of adding a 6-methyloctanoyl as well as an octanoyl group to the N terminus of specific LF11-derived peptides in terms of membrane perturbation and antimicrobial as well as hemolytic activity. The results lead to two separate models of interactions for the non-acylated and *N*-acylated peptide types.

EXPERIMENTAL PROCEDURES

Lipids and Peptides—1,2-Dipalmitoylphosphatidylglycerol (sodium salt) (DPPG), 1-palmitoyl-2-oleoyl-*sn*-glycero-3-phosphoethanolamine (POPE), and *E. coli* total membrane lipid extract (58% phosphatidylethanolamine (PE), 15% phosphatidylglycerol, 10% cardiolipin, and 17% other) were purchased from Avanti Polar Lipids, Inc., and used without further purification. Purity (>99%) was checked before and after experiments by thin layer chromatography using $CHCl_3/CH_3OH/NH_3$ (25% in water) (65:25:5, v/v/v) as mobile phase and detection with molybdenic acid, a phosphorus-sensitive reagent (16).

Peptides in their amidated form (see Table 1) were purchased from PolyPeptide Laboratories, San Diego. The purities were >75% as determined by RP-HPLC. Peptides were dissolved in phosphate-buffered saline (PBS, 20 mM NaP_i, 130 mM NaCl, pH 7.4) at a concentration of 3 mg/ml before each experiment.

Assays for Antimicrobial and Hemolytic Activity—The antimicrobial activity of peptides against *E. coli* ATCC 25922 ($5{\cdot}10^5$ colony-forming units/ml) was tested using susceptibility microdilution assays according to approved guidelines from the National Committee for Clinical Laboratory Standards, and hemolytic activity against human red blood cells was determined as described elsewhere (5). All assays were performed in duplicate and three times.

Preparation of Liposomes for DSC and X-ray—Aqueous dispersions of lipids of 0.1 and 5% weight in PBS buffer for DSC and x-ray, respectively, were prepared before measurement in the presence (lipid-to-peptide molar ratio of 25:1) and absence of peptides as described elsewhere (6, 17, 18).

DSC—DSC experiments were performed with a differential scanning calorimeter (VP-DSC), from MicroCal, Inc. (Northampton, MA). Samples were degassed before measuring. Heating scans were performed at a scan rate of 30 °C/h with a final temperature ~10 °C above the main transition temperature (T_m) and cooling scans at the same scan rate with a final temperature about 20 °C below T_m. The heating/cooling cycle was repeated twice; pre-scan thermostating was allowed for 15 min for the heating scans and 1 min for the cooling scans. Enthalpies were calculated by integrating the peak areas after normalization to phospholipid concentration and base-line adjustment using the MicroCal Origin software (VP-DSC version).

Small Angle X-ray Scattering (SAXS)—X-ray diffractograms were recorded with a SWAX camera (HECUS X-ray Systems, Graz, Austria), which was mounted on a sealed tube Seifert generator (Ahrensburg, Germany) operating at 2 kilowatts. The x-ray beam was filtered for CuK_α radiation ($\lambda = 1.54$ Å) using a nickel foil and a pulse-height discriminator, built into the detection system. The scattered intensity was recorded with a linear position-sensitive detector (HECUS X-ray Systems, Graz, Austria) in the small angle regime of 5×10^{-3} Å$^{-1} < q < 0.5$ Å^{-1}, where $q = 4\pi\sin(\theta)/\lambda$ is the modulus of the scattering wave vector. Calibration in the small angle region was performed with a silver stearate standard. Samples were loaded into thin walled quartz capillaries that were thermally equilibrated for 10 min before initiating data acquisition. Temperature was controlled with an accuracy of 0.1 °C with a programmable Peltier unit. Scattering patterns were recorded at each temperature for 7200 s.

To determine the phosphate-to-phosphate distance (d_{PP}), background-corrected SAXS patterns were analyzed at 25 °C in terms of a global analysis technique, described by Pabst *et al.* (19, 20). The lattice spacings of the cubic phases Pn3m and Im3m were calculated according to Seddon (21).

Fluorescence Spectroscopy and Leakage of ANTS/DPX—Leakage of aqueous contents from large unilamellar vesicles (LUVs) composed of total *E. coli* lipid extract upon incubation with peptide were determined using the 8-aminonaphthalene-1,3,6-trisulfonic acid/*p*-xylene-bis-pyridinium bromide (ANTS/DPX) assay (22). Lipid films (20 mg) were hydrated with 1 ml of 12.5 mM ANTS, 45 mM DPX, 68 mM NaCl, 10 mM HEPES, pH 7.4, following the standard hydration protocol (see above). Subsequently, the dispersions were extruded 20 times through a polycarbonate filter (Millipore-Isopore™) of 0.1 μm pore size to obtain LUVs. The ANTS/DPX containing vesicles were separated from the free ANTS/DPX by exclusion chromatography using a column filled with Sephadex™ G-75 (Amersham Biosciences) fine gel swollen in an iso-osmotic buffer (10 mM HEPES, 140 mM NaCl, and 1 mM EDTA). Phospholipid concentration was determined by phosphate analysis (23). Unilamellarity and size were tested by x-ray and dynamic light scattering, respectively. Fluorescence spectra were obtained at 37 °C (physiological temperature) using an excitation wavelength of 360 nm, an emission wavelength of 530 nm, and a slit width of 5 nm for both excitation and emission monochromators. The fluorescence measurements were performed in quartz cuvettes in 2 ml of the iso-osmotic buffer at the referred temperature. Lipids were diluted to a final concentration of 50 μM. Fluorescence emission was recorded as a function of time before and after the addition of incremental amounts of peptide. The fluorescence increase due to leakage and subsequent dilution of dye was measured after addition of peptides in three concentrations of 2, 4, and 8 μM, corresponding to peptide to lipid molar ratios of 1:25, 1:12.5, and 1:6.25, respectively. The measurements were performed on a SPEX Fluoro Max-3 spectrofluorimeter (Jobin-Yvon, Longjumeau, France) combined with Datamax

software. Data are presented in terms of fluorescence intensity (I_F) in Equation 1,

$$I_F = \frac{F - F_0}{F_{max} - F_0} \quad \text{(Eq. 1)}$$

where F is the measured fluorescence, F_0 is the initial fluorescence without peptide, and F_{max} is the fluorescence corresponding to 100% leakage gained by addition of 1% Triton X-100.

Transmission Electron Microscopy (TEM)—E. coli ATCC 25922 in the exponential phase grown in LB broth were washed, suspended in 10% LB, 90% 20 mM HEPES, pH 7.0, and adjusted to a density of 5×10^8 colony-forming units/ml. Peptides, dissolved in 0.01% acetic acid, were added to 1 ml of bacterial suspension (final peptide concentration 16 μg/ml and 128 μg/ml) and incubated under constant shaking for 30 min at 37 °C. Incubation of bacteria in the presence of 0.01% acetic acid served as a control. An aliquot of the bacterial suspensions was used to determine bacterial viability. Therefore, the aliquot was plated out on agar plates in several dilutions and incubated overnight at 37 °C, and emerging colonies were counted.

For electron microscopic analysis, the bacteria were fixed using 2% osmium tetroxide for 1.5 h (24). After fixation, the samples were washed three times with distilled water. The post-fixation positive stain was carried out with a 2% aqueous uranyl acetate solution (1 h), and the washing procedure was repeated. The material was then dehydrated in a series of ethanol washes (30, 50, 70, 90, and 100%), each for 15 min. The material was transferred to propylene oxide for 15 min. All above mentioned procedures were carried out at room temperature. Infiltration of the samples was done overnight in a 1:1 propylene oxide/Epon/resin mixture at 4 °C. The samples were then embedded in Epon/resin, and polymerization was carried out overnight at 60 °C. Ultrathin sectioning (80–100 nm) was performed with a diamond knife, using a pyramytom. The slices were placed on a copper grid (400 squares) and counter-stained with lead citrate in a CO_2-free environment. Pictures were taken with the EM Zeiss 910.

Stimulation of Human Mononuclear Cells (MNC) by LPS—Lipopolysaccharide (LPS) from *Salmonella enterica* (serovar Minnesota) strain R60 (LPS Ra) was extracted by the phenol/chloroform/petrol ether method (25) from bacteria grown at 37 °C, purified, and lyophilized. For the preparation of aggregates, LPS was dispersed in 20 mM HEPES, pH 7.0, by vortexing, sonicated in a water bath at 60 °C for 30 min, cooled down to room temperature, and subjected to three or four cycles of heating to 60 °C and cooling down to room temperature. After that procedure, the LPS dispersion was stored at least 12 h at 4 °C before use.

MNC were isolated from heparinized blood of healthy human donors as described previously (26). The cells were resuspended in medium (RPMI 1640 medium, 4% human serum) and their number was equilibrated to 5×10^6 cells/ml. For stimulation, 200 μl of MNC (1×10^6 cells) were transferred into each well of a 96-well culture plate. LPS and peptide/LPS mixtures at a weight ratio of 1000:1 were incubated for 30 min at 37 °C and added to the cultures at 20 μl per well (final concentration of LPS is 1 ng/ml). The cultures were incubated for 4 h at 37 °C under 5% CO_2. Supernatants were collected after centrifugation of the culture plates for 10 min at 400 × *g* and used for the immunological determination of TNFα in a Sandwich ELISA using a monoclonal antibody against TNFα (clone 6b from Intex AG, Switzerland) as described earlier (27).

RESULTS

Improved Antimicrobial Activity by Amino Acid Mutation and N-Acylation of LF11—A set of peptide variants were generated based on the LF11 defined and unique fold in lipidic environment (28) with the aim of improving the low antimicrobial activity of LF11 ($MIC_{E.\ coli} > 250$ μg/ml). Thus, deletion of noncharged polar residues that do not contribute to favorable interactions with anionic lipids, main components of bacterial membranes, led to increased antimicrobial activity (Table 1). Single Gln^2 deletion and modification of the C-terminal part (exchange of Val^{10} by Trp (LF11–315) or Lys^9, Val^{10} by Ile, and Arg (LF11–313)) only moderately improved the antimicrobial activity toward *E. coli* ($MIC_{E.\ coli} = 125$ μg/ml). However, further double deletions of the polar residues Gln^4 and Asn^6 in both peptides, now termed LF11–321 and LF11–215, resulted in a marked decrease of their $MIC_{E.\ coli}$ (≤ 32 μg/ml). Furthermore, peptide LF11–322 showed comparable activity to LF11–215, from which it differs only by an additional proline residue at the N terminus. Proline was introduced to provide a rapid and efficient acid-labile Asp-Pro bond for its isolation from the fusion protein, if produced by recombinant techniques (29). The structure of this peptide in lipidic environment was recently solved showing that Pro forms an essential part of the hydrophobic cluster with Phe^2 or Trp^3 (29), which has a similar function on the structural organization of the peptide as the acyl chain of the lipopeptide *N*-lauryl-LF11 (30).

The two most active peptides (LF11–215 and LF-322) as well as a moderately active peptide (LF11–315) were selected to study the effect of *N*-acylation with 6-methyloctanoic acid (PMB-mimic) or octanoic acid. In agreement with our premises, *N*-acylation resulted in either improved (LF11–315 and LF11–215) or similar (LF11–322) activity against *E. coli* (Table 1). Finally, insertion of an additional Phe at position 2 (LF11–324) yielded a peptide being as active as the most potent *N*-acylated peptides because of the highly hydrophobic N-terminal part.

The calculated hydrophobicity of peptides expressed as transfer free energy from water to *n*-octanol (ΔG_{woct}) (31) reflects the peptide propensity to enter the membrane hydrocarbon core and correlates roughly with the antimicrobial activity against *E. coli* (Table 1). The variations in ΔG_{woct} values for the nonacylated peptides whose net charge is +5 show that a certain hydrophobicity threshold is needed for efficient partitioning of these peptides in a bacterial membrane. Deletion of Gln^2 decreasing ΔG_{woct} from 9.5 kcal/mol (LF11) to 7.1 kcal/mol (LF11–315 and LF11–313) is apparently insufficient to significantly improve antimicrobial activity. However, further deletion of the polar residues Gln and Asn in these peptides yielded a calculated transfer free energy value of about 5.5 kcal/mol resulting in peptides (LF11–321, LF11–215) with a high experimentally determined antimicrobial activity against

TABLE 1
Primary structure, hydrophobicity, and biological activity of the parent peptide LF11 and its derivatives

peptide designation	N-acyl group	amino acid sequence [a]	net charge	ΔG_{woct} [b] [kcal/mol]	$MIC_{E.\ coli}$ [c] [μg/ml]	% lysis of 2.5% RBCs [d]
LF11		F Q W Q R N I R K V R-NH_2	+5	9.54	>250	0
LF11-315		F W Q R N I R K **W** R-NH_2	+5	7.14	125	0
6-MO-LF11-315	6-methyl-octanoyl	F W Q R N I R K **W** R-NH_2	+4	n.c.	62	42
LF11-321		F W R I R K **W** R-NH_2	+5	5.52	32	21
LF11-313		F W Q R N I R **I R** R-NH_2	+5	7.12	125	0
LF11-215		F W R I R **I R** R-NH_2	+5	5.50	16-32	1
6-MO-LF11-215	6-methyl-octanoyl	F W R I R **I R** R-NH_2	+4	n.c.	10	17
O-LF11-215	octanoyl	F W R I R **I R** R-NH_2	+4	n.c.	10	12
LF11-322		**P** F W R I R **I R** R-NH_2	+5	5.64	8-16	2
6-MO-LF11-322	6-methyl-octanoyl	**P** F W R I R **I R** R-NH_2	+4	n.c.	8-16	20
LF11-322RR		**P** F W **R R R** I R **I R** R-NH_2	+7	9.26	62	0
LF11-324		**P F** F W R I R **I R** R-NH_2	+5	3.93	8	10

[a] Substitutions and additional amino acids are given in boldface.
[b] Peptide hydrophobicity expressed as transfer free energy of peptides from water to *n*-octanol (ΔG_{woct}) was calculated from the whole residue hydrophobicity scale taking into account the contribution of the C-terminal amide (44). n.c. means not calculated.
[c] MICs against *E. coli* ATCC 25922 were determined as a peptide concentration resulting in less than 2% growth following an overnight incubation in Mueller Hinton medium at 37 °C in the presence of 5×10^5 colony-forming units/ml.
[d] Percentage of hemolysis of human RBCs was calculated following a 1-h incubation at 37 °C in PBS using 1% Triton as 100% lysis and PBS as 0% lysis; peptide concentration was 500 μg/ml.

E. coli, which was most prominent for LF11–324 exhibiting the lowest ΔG_{woct} value (3.93 kcal/mol). However, increasing the affinity to the negatively charged membrane surface by increasing the number of Arg residues (LF11–322RR, +7) yielded only a moderately active peptide, which is in agreement with the transfer free energy being very similar to the mother peptide LF11.

Although the peptide amino acid stretch is too short for the formation of a stable helix, peptide LF11–322 was found earlier to form a helical turn between residues 3 and 6 in the presence of SDS micelles (29). As depicted in Fig. 1 using a helical wheel presentation, the nonacylated peptides do not form a lateral amphipathic structure with a well defined hydrophobic angle. In particular, the highly active peptides LF11–322 or LF11–324 exhibit a more or less equal distribution of hydrophobic and hydrophilic amino acids on a potential helical wheel. The amphipathic moment for these two peptides lies along the "helical axes" with a strongly hydrophobic N-terminal and a highly cationic C-terminal part, as deduced from two-dimensional NMR experiments (29). Of note, Yang *et al.* (32) reported that the ability of bovine lactoferrin-derived peptides to adopt a lateral amphipathic conformation appears less critical to their antimicrobial activities, implying that a higher flexibility or number of active conformations was tolerated for the peptides to exert a high antimicrobial activity. The increase in antimicrobial activity observed in these studies upon *N*-acylation or insertion of hydrophobic residues demonstrates that the driving force for perturbation of the membrane is the hydrophobic N-terminal anchor rather than a defined conformation.

Strengthening the peptide hydrophobicity resulted in slightly reduced cell specificity, as demonstrated by a weakly increased hemolytic activity by the *N*-acylated peptides as well as by the most hydrophobic nonacylated peptide, LF11–324 (Table 1). In addition, LF11–321, although characterized by a lower hydrophobicity than LF11–324, also induced to some degree lysis of human red blood cells. This finding may be explained by the presence of an additional tryptophan residue, as building synthetic combinatorial libraries around an amphipathic α-helical peptide revealed a correlation between the presence of tryptophan residues and increase of hemolytic activity (33). No lysis of human red blood cells was observed for the antimicrobial weakly active peptides (LF11, LF11–313, and LF11–315). The fact that LF11–315 does not exhibit hemolytic activity, although it contains two tryptophan residues like LF11–321, reflects that the threshold of peptide hydrophobicity is needed to be able to penetrate into a cell membrane (see Table 1).

Correlation between Effects on Model Membranes and Biological Activity—E. coli cytoplasmic membrane consists of a mixture of negatively charged and neutral lipids like phosphatidylglycerol (6%) and PE (82%) (34), where palmitic (C16:0) and oleic acid (C18:1) account for the major fatty acids of the phospholipids (35). Therefore, liposomes composed of the disaturated DPPG and the mixed chain POPE, respectively, were used as simple membrane mimic to study the effect of LF11-derived peptides on lipid bilayers. Additional experiments on selected peptides were also performed using liposomes composed of *E. coli* total lipid extracts.

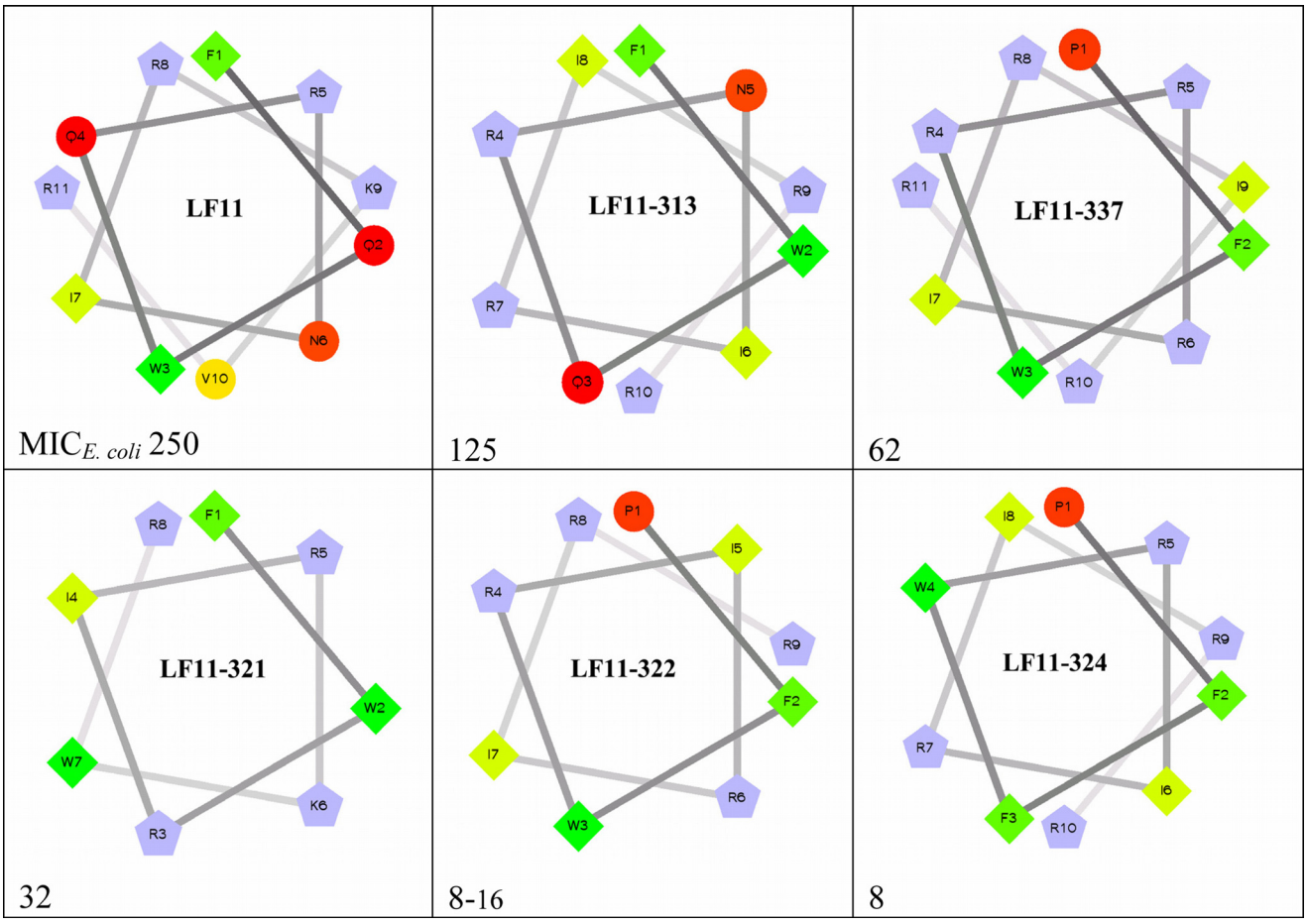

FIGURE 1. **Helical wheel projection of LF11 and peptides derived from them.** Respective values of MIC$_{E.\ coli}$ are indicated in the *left corner*. Hydrophilic residues are represented as *red circles*; potentially positively charged as *blue pentagons,* and hydrophobic residues as *green diamonds*. The intensity of the *green* color decreases proportionally to the hydrophobicity.

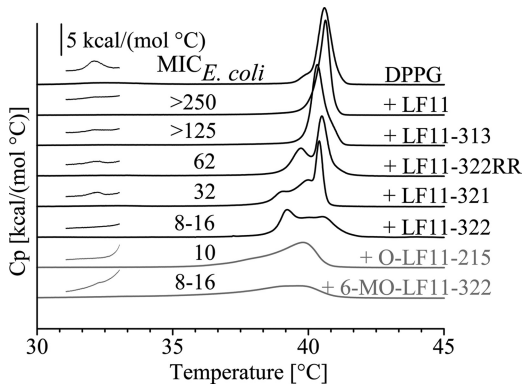

FIGURE 2. **DSC thermograms of DPPG in the absence and presence of peptides (25:1, lipid-to-peptide molar ratio).** For clarity, the DSC curves were displayed on the *ordinate* by arbitrary units. The pre-transition is shown enlarged. Scan rate was 30 °C/h. *N*-Acylated peptides are shown in *gray*. For analyzed data see Table 2.

Calorimetric Studies Using DPPG Liposomes and Electrostatic Interactions—The thermotropic phase behavior of DPPG shows two phase transitions (Fig. 2; Table 2), which can be attributed to the pre-transition from the lamellar gel ($L_{\beta'}$) to the ripple phase ($P_{\beta'}$) at 32.5 °C and the main or chain-melting transition from the $P_{\beta'}$ to the fluid phase (L_{α}) at 40.6 °C (36, 37). As reported earlier (6), addition of LF11 at a lipid-to-peptide molar ratio of 25:1 resulted in a decrease of the pre-transition enthalpy (ΔH_{pre}), whereas the main transition was unaffected. The presence of peptides exhibiting slightly higher antimicrobial activity than LF11 (LF11–313 in Fig. 2) led also to a decrease in ΔH_{pre} and additionally to a minor decrease of the main transition temperature (T_m) without affecting its half-width ($\Delta T_{½}$) (Fig. 2 and Table 2). This indicates a weak destabilization of the gel phase by such peptides. In contrast, the presence of nonacylated peptides, which exhibited higher antimicrobial activities toward *E. coli* (MIC ≤62 μg/ml), resulted in overlapping transitions in the main transition region. Two clearly separated endothermic peaks were only detected in the presence of LF11–322RR, which is rich in arginine residues, including a three consecutive Arg residue stretch. Deconvolution of LF11–322RR thermogram suggests that these peaks can be attributed on the one hand to peptide-poor (unaffected) DPPG domains melting close to the main transition temperature of pure DPPG and on the other hand to peptide-enriched (affected) DPPG domains, which melt at lower temperature (Table 2). Interestingly the half-width of both transitions was similar indicating that the lipid domains undergoing the cooperative chain-melting transition are of similar size. The ratio of their respective transition enthalpies suggests that about 40% of DPPG was affected by LF11–322RR (Table 2). The magnitude of peptide-enriched domains increased at the expense of peptide-unaffected domains in the presence of peptides exhibiting

TABLE 2

Thermodynamic parameters of DPPG in the absence and presence of LF11 and derived peptides at a lipid-to-peptide molar ratio of 25:1

The abbreviations used are as follows: pr, peptide-enriched; pp, peptide-poor.

	ΔH_{pre}	T_{pre}	$\Delta H_{m\ pr}$	$T_{m\ pr}$	$\Delta T_{½\ pr}$	$\Delta H_{m\ pp}$	$T_{m\ pp}$	$\Delta T_{½\ pp}$
	kcal/mol	*°C*	*kcal/mol*	*°C*	*°C*	*kcal/mol*	*°C*	*°C*
DPPG	1.2	32.5				9.1	40.6	0.56
LF11	0.2	32.6				9.6	40.6	0.55
LF11–313	0.2	32.6				9.8	40.3	0.55
LF11–322RR	0.7	32.8	3.9	39.7	0.66	6.1	40.5	0.47
LF11–321	0.8	32.9	3.0/3.8	39.1/40.0	1.4/1.0	2.6	40.4	0.4
LF11–322	0		3.2/2.9	39.2/40.0	0.8/1.4	2.2	40.5	0.9
O-LF11–215	0		10.3	39.8	1.9			
6MO-LF11–322	0.2	33.6	8.6	39.6	3.1			

higher antimicrobial activity (lower MIC values) as shown, *e.g.* for LF11–321 and LF11–322. In addition, these peptides gave rise to multiple overlapping transitions. Their thermodynamic parameters calculated by deconvolution of the thermograms demonstrated the occurrence of two peptide-enriched domains at lower temperatures (Table 2). The magnitude of $\Delta T_{½}$ for the peptide-enriched domains also increased indicating a smaller domain size as compared with pure DPPG.

In contrast to the clearly resolved overlapping endothermic peaks in the presence of nonacylated peptides, *N*-acylated peptides, as shown exemplarily for 6-MO-LF11–322 and O-LF11–215, induced a broad asymmetric main transition at lower temperatures (Fig. 2 and Table 2), *i.e. N*-acylated peptides did not induce segregation into peptide-enriched and peptide-poor lipid domains. Moreover, the shape and width of these endotherms clearly indicated the occurrence of a very low cooperative phase transition suggesting that the chain melting occurs sequentially in many small lipid domains. Overall, these results show that the extent of perturbation on the negatively charged bacterial mimic membrane qualitatively correlates with the peptides antimicrobial activity.

Calorimetric and X-ray Studies Using POPE Liposomes and Hydrophobic Interactions—Because of their cone-shaped molecular geometry, PEs are able to form nonlamellar structures particularly the inverse-hexagonal (H_{II}) phase (38). Therefore, peptide-lipid interaction with PEs can also yield information on the impact of peptides on the formation of nonlamellar structures. To observe the lamellar gel (L_{β}) to fluid (L_{α}) and the lamellar to inverse-hexagonal phase transition in an equitable temperature range, liposomes composed of a mixed chain PE, namely POPE, were used.

In agreement with previously published work (38), a sharp main transition was observed for pure POPE at T_m = 25.5 °C (ΔH_m = 4.5 kcal/mol) and a broader lamellar to inverse hexagonal phase transition at T_{HII} = 76.7 °C (ΔH_{HII} = 0.3 kcal/mol). Fig. 3 shows as an example the excess heat capacity curves of POPE obtained in the presence of LF11–322 and its 6-MO-derivative, respectively. Addition of the nonacylated peptide had no effect on the main transition, whereas T_m decreased by ~0.5 °C and ΔH_m by ~50%, when the *N*-acylated peptide was added. This resembles the effect of the frog skin antimicrobial peptide PGLa (18), which may also perturb the gel phase of POPE by insertion of its more flexible hydrophobic N-terminal part (37).

In contrast to their different effect on the main transition, both LF11–322 and 6-MO-LF11–322 abolished the L_{α}-H_{II} phase transition in the temperature range studied (up to 90 °C). This was confirmed by x-ray measurements showing only Bragg peaks being indicative for correlated bilayers in the L_{α} phase (Fig. 3, *inset*). For comparison, a respective typical H_{II} pattern of POPE in the absence of peptide is shown in Fig. 3, *inset*. Thus, it is obvious that both peptides stabilize the fluid L_{α} bilayer phase of POPE. At a first glance, this observation may seem to be contradictive to the different effect of nonacylated and *N*-acylated peptides on the chain-melting transition. If one considers, however, that the peptide amphipathic moment lies along the helical axes (29), incorporation of the peptide perpendicular into the bilayer interface would enable an optimal penetration of the hydrophobic N-terminal residues into the hydrophobic core of the lipid bilayer. Penetration of the three N-terminal residues (PFW in LF11–322; Trp preferentially locates at the membrane interface (39)) does not apparently induce a significant perturbation of the lateral hydrocarbon chain packing in POPE bilayers. This may be explained by the cone-shaped molecular geometry of this phospholipid that complements the molecular shape of the peptide. Such a localization of the peptide would fill the gaps in the headgroup region of a planar PE bilayer and therefore also prevent the formation of negatively curved structure such as the H_{II} phase. However, the *N*-acyl chain penetrates deeper into the hydro-

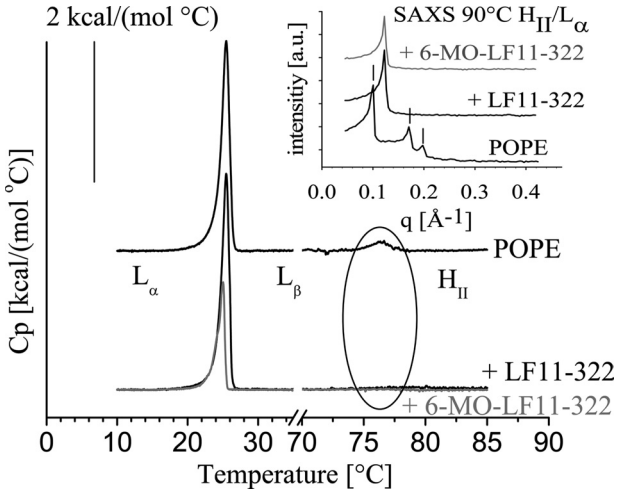

FIGURE 3. **DSC thermograms of POPE in the absence and in the presence of peptides (25:1, lipid-to-peptide molar ratio).** For clarity, the DSC curves were displaced on the *ordinate* by arbitrary units. Scan rate was 30 °C/h. *N*-Acylated peptides are shown in *gray*. Phase transition from L_{α} to H_{II} is *highlighted*. *Inset,* SAXS diffraction pattern in the absence and presence of peptide at 90 °C. POPE displays the typical pattern of H_{II} phase (lines indicating the Bragg peaks at *q* values of 0.099, 0.171, and 0.197 $Å^{-1}$). In the presence of peptides the lipid is in the fluid phase.

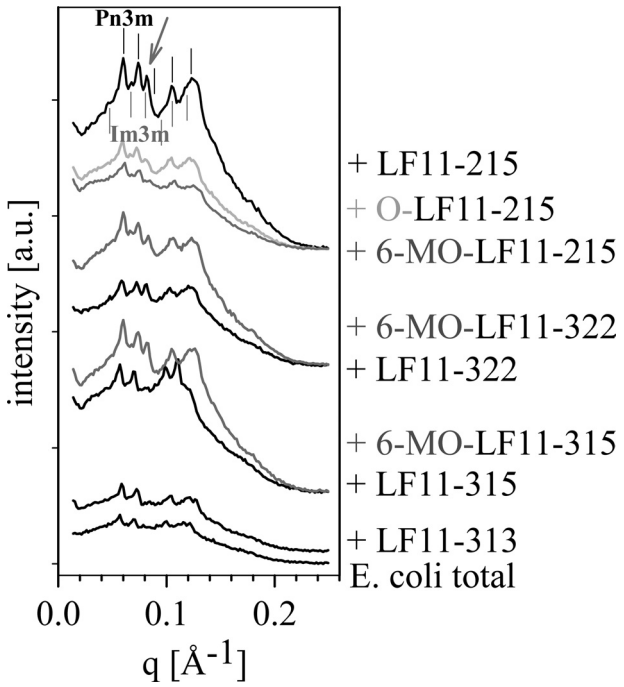

FIGURE 4. **SAXS patterns of an aqueous dispersion of *E. coli* membrane total lipid extract at 25 °C after one heating/cooling cycle (25/85/25 °C).** Position of the *hkl* reflections corresponding to a cubic phase of space group Pn3m are indicated by perpendicular *black lines* and of space group Im3m by *gray lines*. *Arrow* indicates the third order peak of Im3m. For corresponding lattice spacing see Table 3.

TABLE 3

Deviation of structural parameters of the fluid phase of *E. coli* total lipid extracts at 25 °C and of the respective cubic phases after one heating-cooling cycle in the presence of LF11-derived peptides (lipid-to-peptide molar ratio of 25:1

Structural parameters for *E. coli* total lipids in the absence of peptides are as follows: phosphate-to-phosphate distance, d_{pp} = 40.5 Å; lattice spacing, Pn3m = 151 Å and Im3m = 194 Å. ND means not detected.

Sample	Δd_{pp}	Δ lattice spacing, Pn3m	Δ lattice spacing, Im3m
	Å	Å	Å
LF11–315	−0.1	+2	ND
6-MO-LF11–315	0	−9	−11
LF11–313	0	−3	ND
LF11–215	−0.3	−9	−9
6-MO-LF11–215	+1.5	−11	−14
O-LF11–215	+0.2	−5	−8
LF11–322	−0.4	−5	−8
6-MO-LF11–322	+0.4	−9	−13
LF11–324	−0.7	−7	−9

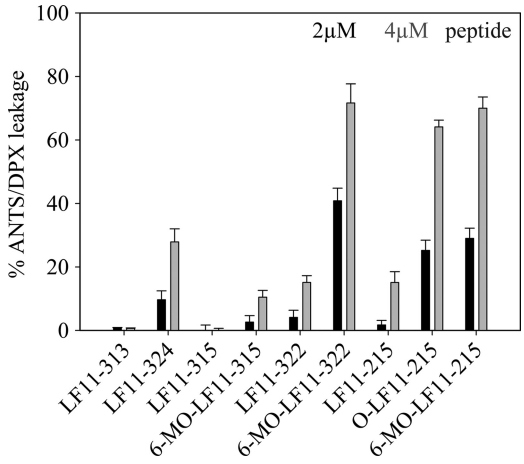

FIGURE 5. **Induction of ANTS/DPX leakage of LUVs of *E. coli* membrane lipids (50 μM) in the presence of 2 μM peptide (*black bars*) and 4 μM peptide (*gray bars*) at 37 °C.**

phobic core of POPE interfering with the lateral hydrocarbon chain packing and thereby inducing a disorder, which leads to a destabilization of the gel phase and consequently to a decrease of the transition enthalpy and temperature. However, in terms of H_{II}-phase formation, the molecular geometry of the *N*-acylated peptides may also be described by an inverse cone because of the flexible acyl chain. This would complement the cone-shaped geometry of the POPE lipid resulting in stable planar bilayers. PGLa was also shown to stabilize the liquid crystalline phase of POPE bilayers, although to a minor extent (18). It should be noted that in contrast to these observations, the antimicrobial peptide NK-2 decreased the onset temperature of the L_{α}-H_{II} phase transition (40), emphasizing different modes of lipid-peptide interactions that will give rise to different killing mechanism at the molecular level (7).

Effect of Peptides on E. coli Membrane Lipids, Bilayer Thickness, Membrane Spontaneous Curvature, and Permeability—After gaining information on the effect of the peptides on bacterial membrane mimics composed of single lipid components, their effects on liposomes composed of *E. coli* total lipid extracts were studied (Fig. 4). In an earlier study, we have already demonstrated a correlation between the antimicrobial activity of the nonacylated peptides LF11–313 and LF11–324 (there termed VS1–13 and VS1–24) and their ability to induce membrane curvature strain as well as bilayer thinning in *E. coli* lipid model membranes using small angle x-ray scattering (9).

In agreement with these earlier findings, a deviation of the bilayer thickness of the physiologically relevant fluid phase of *E. coli* total lipid extracts was observed at 25 °C (SAXS pattern not shown) for all active peptides studied, although weakly active peptides, like LF11–313 and LF11–315, had no effect on the bilayer thickness (Table 3). The active nonacylated peptides showed a small but significant decrease of the phosphate-to-phosphate distance of the opposing lipid monolayers (d_{PP}). The bilayer thinning was most prominent for the highly active LF11–324, which is consistent with previously published results (9). Again, the *N*-acylated peptides exerted a different effect inducing an average increase of the bilayer thickness, whereby the largest deviation was observed for 6-MO-LF11–215 (increase of d_{PP} by 1.5 Å). It should be noted that these values are averaged values over the whole bilayer, which means that locally at the side of peptide insertion the thinning or thickening effect will be larger. This can significantly affect the bilayer stability and permeability properties because of the creation of defects between these laterally structurally diverse lipid domains.

Therefore, to test the permeability of this model system, we prepared large unilamellar vesicles composed of *E. coli* lipids loaded with ANTS/DPX and incubated them with the peptides at 37 °C. This allowed us to pursue the effect of peptides at a physiological temperature, where the *E. coli* lipid extract is in the fluid phase. Vesicles incubated with the biologically weakly active peptides LF11–313 or LF11–315 at a lipid-to-peptide molar ratio of 25:1 and 12.5:1 promoted only negligible release of the trapped fluorescence marker (Fig. 5), even when the pep-

tide concentration was increased to yield a lipid-to-peptide molar ratio of 6.25:1 (data not shown). The 6-MO-derivative of LF11–315 showed improved leakage potency but was still less effective than the more active nonacylated peptides LF11–215, LF11–322, and LF11–324. This also correlates with the fact that the 6-MO-LF11–315 peptide did not alter the bilayer thickness resulting in less defects in contrast to the bilayer thinning observed in the presence of the active nonacylated peptides. Among the nonacylated peptides, LF11–324, the biologically most active and hydrophobic peptide, was also the most efficient in inducing a significant ANTS/DPX release (up to 30%). This can be explained by the strongest bilayer thinning (−0.7 Å) causing most severe membrane perturbation because of line defects arising at the peptide-enriched and peptide-poor domains, which will differ significantly in their bilayer thickness.

Besides 6-MO-LF11–315, the *N*-acylated peptides induced a much higher release of ANTS/DPX (~70% at a lipid-to-peptide molar ratio of 12.5:1) as compared with their nonacylated counterparts. This seems to be due to the larger number of defect lines as can be deduced from calorimetric experiments, which yield much smaller domain sizes for the *N*-acylated peptides in case of DPPG.

Interestingly, LF11–324 was only half as efficient in terms of permeability increase as compared with the *N*-acylated peptides derived from LF11–215 and LF11–322, although it has even a slightly lower $MIC_{E.\ coli}$ value. To understand this seemingly contradictive result in terms of correlating antimicrobial activity and vesicle leakage, one has to consider that the membrane of *E. coli* consists of two bilayers, where the outer leaflet of the outer membrane almost exclusively consists of anionic LPS. As shown previously (41, 42), *N*-acylation of LF11 led to an increase in LPS binding. Therefore, we measured the LPS-induced production of TNFα in human MNCs and its inhibition due to peptide binding to LPS. Indeed, *N*-acylation of LF11–215 and LF11–322 markedly decreased TNFα production reflecting enhanced binding to LPS (Fig. 7, *bottom panel*). This elevated level of peptide binding to LPS might counteract their increased membrane permeabilizing properties (Fig. 7, *middle panel*), and therefore, no improvement in antimicrobial activity was observed (Fig. 7, *top panel*). This view was supported by the finding that *N*-acylation of LF11–315 did not result in elevated LPS binding but enhanced antimicrobial activity in accordance with the increased permeability (Fig. 7). The impact of these observations will be discussed in more detail later.

We also evaluated the effect of these peptides on the cubic phases of *E. coli* lipid extract that form at elevated temperatures (Fig. 4 and Table 3). Lipid extracts from *E. coli* membranes have been shown to adopt two coexisting cubic phases belonging to the space groups Pn3m and Im3m (9, 17). For all peptides studied, a decrease of the onset temperature of cubic phase formation was observed. Although the weakly active LF11–313 and LF11–315 did not significantly decrease the onset temperature, the highly active LF11–324 lowered it by about 20 °C, in agreement with earlier results (9). In the presence of *N*-acylated peptides, the cubic phase formation occurred at about 10 °C below the pure lipid extract (data not shown). In addition, all active peptides affected the fraction of the coexisting cubic phases in favor of Im3m, as indicated by the increased intensity of the third order peak ($\sqrt{6}$) of this space group (indicated by an *arrow* in Fig. 4), and it had a marked effect on the lattice spacing, which was reduced up to 11 Å for Pn3m and 14 Å for Im3m in the case of 6-MO-LF11–215 (Table 3). Such a large reduction of the lattice spacing implies a decreased diameter of the water channels and consequently a decrease of the spontaneous curvature. This can be achieved by a reduction of the headgroup area due to dehydration and/or reorientation of the headgroup because of electrostatic interaction between lipids and peptides. In any case, the peptides obviously induce a curvature strain in the leaflets of this mixed lipid bilayer, which can result in lipid-peptide domains with different structural properties as deduced from the x-ray experiments, thereby destabilizing the bilayer structure and increasing bilayer permeability. The *N*-acylated peptides are more potent in inducing leakage, most probably because of creating more defects than the nonacylated peptides, which rather induce charge segregation arising in larger domains and hence less defect lines. At elevated temperature (in case of LF11–324 close to physiological temperature) the bilayer structure of *E. coli* lipid extracts becomes energetically unfavorable and transforms into cubic structures.

Effect of Peptides on E. coli Cells in Vitro—Morphological changes of *E. coli* ATCC25922 upon treatment with nonacylated peptides and their *N*-acylated derivatives were visualized by TEM. Viability tests were performed in parallel. Bacteria were treated with peptides at concentrations close to their MIC (16 μg/ml) and considerably above their MIC (128 μg/ml). The observed morphological changes are clear-cut indicators for a membrane-based mode of action. The nonacylated peptide LF11–215 induced membrane ruffling and the detachment of the inner and outer membranes (Fig. 6). These effects were also observed after treatment of *E. coli* with the peptide O-LF11–215. In contrast to the nonacylated peptide, however, O-LF11–215 induced the formation of extrusions of lipid material, presumably from the outer membrane. These extrusions appeared well ordered and of a defined length at the higher peptide concentration (Fig. 6). After incubation of bacteria with peptides, aliquots of the bacterial suspensions were plated out on LB agar plates and incubated overnight. Colony growth of *E. coli* was completely inhibited by 16 μg/ml of O-LF11–215 and reduced by 81% for LF11–215. At 128 μg/ml peptide concentration, no colonies developed in the presence of both peptides. Results from TNFα production experiments (Fig. 7) are fully in line with this observation, which demonstrated that O-LF11–215 indeed exhibited a highly increased LPS neutralization compared with its nonacylated parent peptide because of strong LPS binding.

TEM results clearly underline that the peptide-induced pronounced differences of the bacterial morphology are not due to differences in the antibacterial potency of nonacylated and *N*-acylated peptide pairs but originate from a different mode of membrane interaction. Moreover, those results demonstrate that at MIC a severe membrane effect leads to bacterial killing before visible lysis. Similar results were observed for the peptide pair LF11–322 and 6-MO-LF11–322 (Fig. 6).

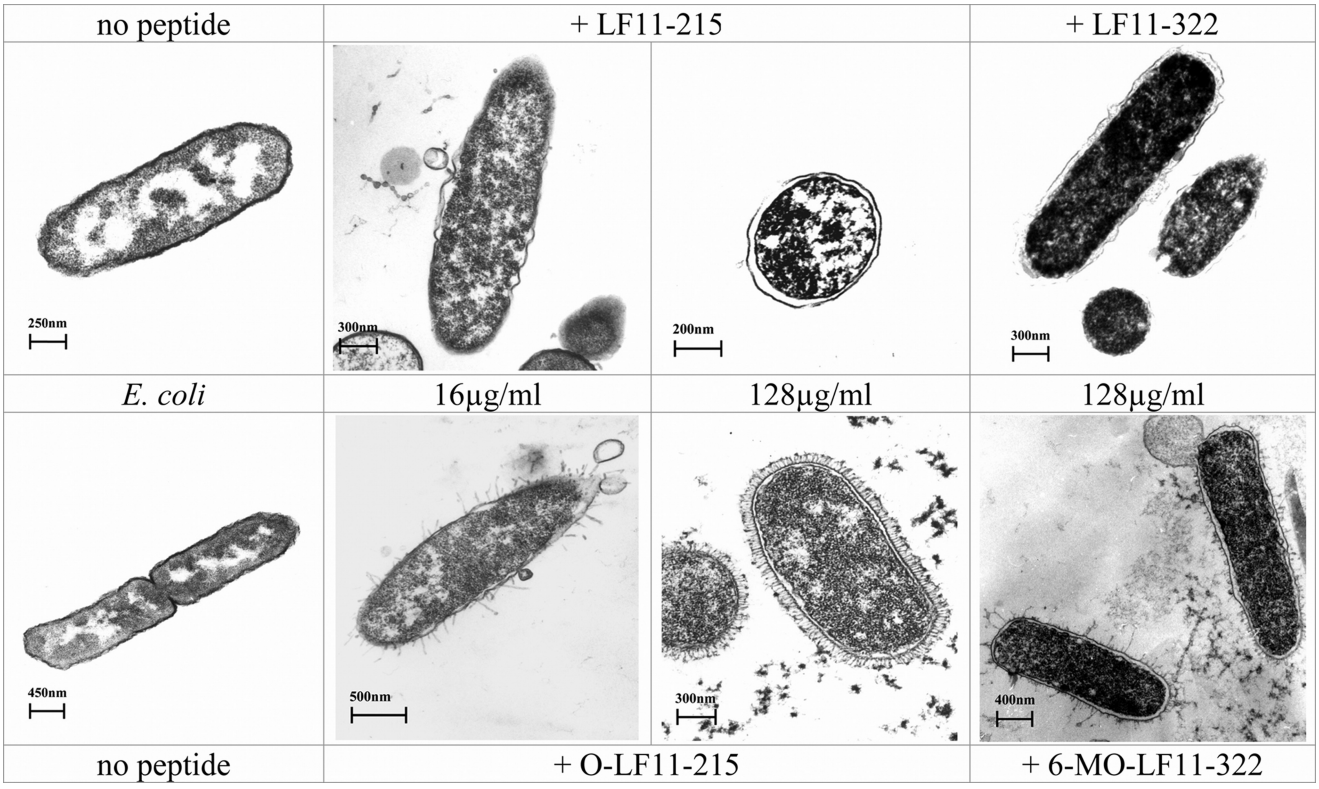

FIGURE 6. **Transmission electron microscopy pictures taken from *E. coli* ATCC25922 in the absence and presence of nonacylated and *N*-acylated peptides near the respective MIC level at 16 μg/ml and above their MIC level at 128 μg/ml; the designation of the peptide is indicated in the panels.**

DISCUSSION

Biophysical studies revealed that on a molecular level nonacylated and *N*-acylated peptides exhibited different effects on the structure of phospholipid model membranes representative for the cytoplasmic membrane of *E. coli*, which is reflected in the following models.

Fig. 8*A* describes the interaction of the nonacylated peptides with *E. coli* membranes as an extension of a model proposed previously (7). The nonacylated peptides strongly interact with negatively charged components of bacterial lipid bilayers forming large domains, which are laterally segregated from peptide-depleted domains. In contrast, bilayers of PE, the dominant neutral phospholipid of *E. coli*, are not significantly affected by incorporation of these peptides, which can be explained by the complementary molecular shape of lipid and peptide (see under "Results").

Insertion of the peptide in the bilayer interface of phosphatidylglycerol, however, creates a "void" in the hydrophobic core, an energetically unfavorable situation, which can be released with a movement of the opposing monolayer toward the peptide and consequently filling this void (7). In turn, this would result in a local thinning of the bilayer as observed for the *E. coli* lipid model system. The coexistence of peptide-enriched and peptide-poor lipid domains characterized by markedly different structural properties is expected to create defects at their domain boundaries, which promotes membrane permeability leading to leakage of cellular content. The different degree of permeability observed for the various nonacylated peptides, *i.e.* leakage induced in *E. coli* lipid vesicles, correlated roughly with their biological activity and can be explained by their different partitioning into the bilayer according to their hydrophobicity (Table 1) and consequently to their ability to induce peptide-enriched membrane domains (Table 2).

Insertion of *N*-acylated peptides, sketched in Fig. 8*B*, has different consequences on the structural integrity of bilayers as compared with their nonacylated parent compounds, whereby we cannot exclude the presence of peptide aggregates because of their higher hydrophobicity. In contrast to their parent peptides, *N*-acylated peptides affect both bilayer components, negatively charged and neutral lipids. Moreover, insertion of the *N*-acylated peptides will not create a void in the hydrophobic core of the bilayer because of the presence of the *N*-acyl chain, which can fill to some extent the space below the peptide. Thus, there is no need for moving the opposing monolayer toward the peptide. Instead packing defects now probably arise from conformational changes of the flexible hydrocarbon chains of the peptide surrounding lipids differing from the bulk phase lipids. Therefore, the minor thickening of the bilayer in the physiologically relevant fluid phase suggests that the *N*-acylated peptide induces some order within the hydrocarbon chains of the lipid. This is in agreement with earlier findings showing that conjugating the N-terminal part of LF11 with lauric acid exhibited a kind of cholesterol-like effect, *i.e.* an increase of fluidity in the gel phase and a decrease of fluidity in the fluid phase of DPPG (6). An extended acyl chain of the lipopeptide, which could fill the space in the hydrophobic core of the membrane, would be primarily expected to increase the affinity of these peptides to the membrane, but not to increase bilayer defects. However, two-dimensional NMR experiments revealed that in negatively charged SDS micelles, the *N*-lauryl chain in LF11 makes a turn

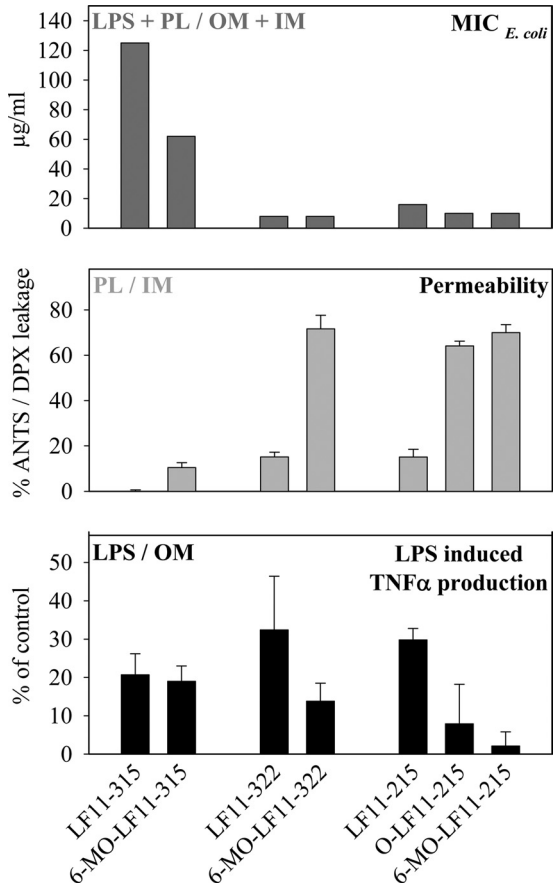

FIGURE 7. **Correlation of $MIC_{E.\ coli}$ with membrane permeabilization and LPS neutralization of nonacylated peptides and their *N*-acylated derivatives (*OM*, outer membrane; *IM*, inner membrane; *LPS*, lipopolysaccharides; *PL*, phospholipids).** *Top panel,* $MIC_{E.\ coli}$ values (taken from Table 1) reflecting the interaction of peptides with both LPS and phospholipids. *Middle panel,* interaction of peptides with phospholipids as deduced from membrane permeability measurements of ANTS/DPX leakage from LUVs of *E. coli* membrane lipids (50 μM) in the presence of 4 μM peptide at 37 °C (see also Fig. 5). *Bottom panel,* interaction of peptides with LPS as illustrated from LPS Ra (*S. minnesota* R60) induced TNFα production in human mononuclear cells at 1 ng/ml and its inhibition by nonacylated and *N*-acylated peptides. Values are given as a percentage of control.

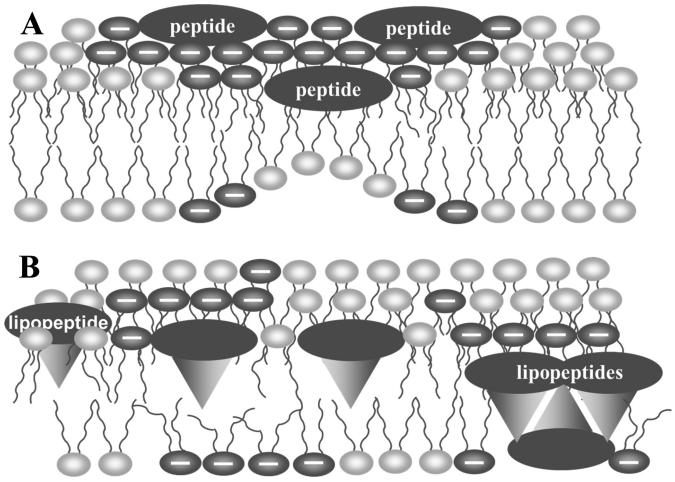

FIGURE 8. **Models recapitulating the differences in peptide-membrane interaction between nonacylated (*A*) and *N*-acylated (*B*) antimicrobial peptides with bacterial cytoplasmic membranes, including neutral and anionic phospholipids.**

toward the peptide backbone forming a kind of a ring structure together with the aromatic residues of Phe^1 and Trp^3, which could mimic to some extent the rigid ring structure of cholesterol (30). Consequently, we can conclude that in the presence of *N*-acylated peptides, the surrounding lipids adopt a different degree of trans-gauche isomerization as compared with the bulk phase lipids giving rise to a lateral heterogeneous bilayer structure consisting of small domains. As a result, the sum of defect lines will be larger in this system as compared with bilayers containing nonacylated peptides and therefore will exhibit higher membrane permeability as observed in the *E. coli* lipids leakage experiments.

According to these observations, one would expect that the *N*-acylated peptides would have a lower MIC value as compared with their nonacylated parent peptide. This seems to be in contradiction with the observed MIC values, which did not differ significantly between highly active nonacylated peptides and their *N*-acylated derivatives. Likewise, Lockwood *et al.* (43) reported that conjugation of SC4 dodecapeptide with fatty acids had only little or no increase in bactericidal activity against Gram-negative bacteria. Obviously, the MIC value reflects the potential interaction of the antimicrobial peptides with both the outer and inner membrane of Gram-negative bacteria (*e.g. E. coli*), which differ significantly in their lipid composition. Although the outer membrane is highly asymmetric with its outer leaflet composed almost exclusively of LPS, the inner cytoplasmic membrane is basically a phospholipid bilayer. Thus, the experimental approaches presented here indicate different levels of interaction (Fig. 7), *i.e.* inhibition of TNFα production in human MNCs reflects the capability to bind to LPS (interaction with components of the outer membrane), although permeability and structural studies on the membrane mimics reflect the ability to interfere with the inner membrane. Therefore, our observations can be explained considering the significantly higher affinity of *N*-acylated peptides to LPS as also shown in earlier studies (41–43). Upon interaction with *E. coli,* a considerable fraction of those *N*-acylated peptides (like O- and 6-MO-LF11–215 and 6-MO-LF11–322) will be captured by LPS decreasing their effective concentration at the inner cytoplasmic membrane, where supposedly the killing event takes place. However, in the case of peptides, where low LPS neutralization is observed, permeability as detected in the model system can be correlated to their MIC value. This is supported by the TEM pictures showing detachment of the outer and inner membrane of *E. coli* for both peptide types but formation of tubular protrusions from the outer membrane only in the presence of *N*-acylated peptides. Therefore, considering the antimicrobial activity of peptides against Gram-negative bacteria differences in the interaction with LPS, the first site of contact has to be taken into account. Moreover, in terms of drug development, it is important to consider the cell membrane selectivity, *i.e.* in a first approach to compare antimicrobial and hemolytic activity. Indeed, our results show that *N*-acylation of peptides induced some lysis of human red blood cells under our experimental conditions (500 μg/ml at 2.5% RBCs). The level of hemolytic activity nevertheless remains within an acceptable range considering that the peptide concentration for the most active peptides, where hemo-

lysis between 10–20% was observed, is still 30–60 times higher than the respective $MIC_{E.\ coli}$. Therefore, peptides with the highest antimicrobial and lowest hemolytic activity such as LF-11–324 or O-LF11–215 are good templates for further development of novel antimicrobial compounds.

In summary, we have demonstrated that acylation of the N-terminal part of lactoferricin-derived peptides leads to a higher effect on all lipid components of the cytoplasmic membrane of *E. coli*. Finally, it can also be concluded that phospholipid model studies can be better correlated to the lethal peptide effect on the cytoplasmic (inner) membrane than to MIC values, which reflect the sum of effects on the outer and inner membrane.

Acknowledgments—We gratefully appreciate the fruitful discussions with Ignacio Moriyón, Guillermo Martinez de Tejada, and Mateja Zorko. We thank Susana Sánchez-Gómez for hemolysis experiments and Kerstin Stephan, Jasmin Tiebach, and Sabine Tumer for technical support.

REFERENCES

1. Sorenson, M., and Sorenson, M. P. (1939) *C. R. Trav. Lab.* **23,** 55–59
2. Masson, P. L., Heremans, J. F., and Dive, C. H. (1966) *Clin. Chim. Acta* **14,** 735–739
3. Masson, P. L., Heremans, J. F., and Schonne, E. (1969) *J. Exp. Med.* **130,** 643–658
4. Wakabayashi, H., Takase, M., and Tomita, M. (2003) *Curr. Pharm. Des.* **9,** 1277–1287
5. Blondelle, S. E., Jerala, R., Lamata, M., Moriyon, I., Brandenburg, K., Andrä, J., Porro, M., and Lohner, K. (2004) in *Peptide Revolution: Genomics, Proteomics & Therapeutics* (Chorey, M., and Sawyer, T., eds) pp. 877–878, Kluwer Academic, Dordrecht, Netherlands
6. Zweytick, D., Pabst, G., Abuja, P. M., Jilek, A., Blondelle, S. E., Andrä, J., Jerala, R., Monreal, D., Martinez de Tejada, G., and Lohner, K. (2006) *Biochim. Biophys. Acta* **1758,** 1426–1435
7. Lohner, K., and Blondelle, S. E. (2005) *Comb. Chem. High Throughput Screen.* **8,** 241–256
8. Lohner, K. (2009) *Gen. Physiol. Biophys.* **28,** 105–116
9. Zweytick, D., Tumer, S., Blondelle, S. E., and Lohner, K. (2008) *Biochem. Biophys. Res. Commun.* **369,** 395–400
10. Sánchez-Gómez, S., Lamata, M., Leiva, J., Blondelle, S. E., Jerala, R., Andrä, J., Brandenburg, K., Lohner, K., Moriyón, I., and Martínez-de-Tejada, G. (2008) *BMC Microbiol.* **8,** 196
11. Wakabayashi, H., Matsumoto, H., Hashimoto, K., Teraguchi, S., Takase, M., and Hayasawa, H. (1999) *Antimicrob. Agents Chemother.* **43,** 1267–1269
12. Strøm, M. B., Haug, B. E., Rekdal, O., Skar, M. L., Stensen, W., and Svendsen, J. S. (2002) *Biochem. Cell Biol.* **80,** 65–74
13. Blondelle, S. E., Jerala, R., Lamata, M., Martinez, D. T., Howe, J., Andrä, J., Porro, M., Deutsch, G., Zweytick, D., and Lohner, K. (2005) in *Proceedings of the 3rd International and 28th European Peptide Symposium* (Flegel, M., Fridkin, M., Gilon, C., and Slaninova, J., eds) pp. 81–82, Kenes International, Geneva, Switzerland
14. Deutsch, G., Zweytick, D., Blondelle, S. E., Monreal, D., Leiva, J., and Lohner, K. (2006) *Biophys. J.* **90,** 1039/B162
15. Ofek, I., Cohen, S., Rahmani, R., Kabha, K., Tamarkin, D., Herzig, Y., and Rubinstein, E. (1994) *Antimicrob. Agents Chemother.* **38,** 374–377
16. Hahn, F. L. (1956) *Pharm. Zentralhalle. Dtschl.* **95,** 309–312
17. Staudegger, E., Prenner, E. J., Kriechbaum, M., Degovics, G., Lewis, R. N., McElhaney, R. N., and Lohner, K. (2000) *Biochim. Biophys. Acta* **1468,** 213–230
18. Hickel, A., Danner-Pongratz, S., Amenitsch, H., Degovics, G., Rappolt, M., Lohner, K., and Pabst, G. (2008) *Biochim. Biophys. Acta* **1778,** 2325–2333
19. Pabst, G., Koschuch, R., Pozo-Navas, B., Rappolt, M., Lohner, K., and Laggner, P. (2003) *J. Appl. Crystallogr.* **36,** 1378–1388
20. Pabst, G., Rappolt, M., Amenitsch, H., and Laggner, P. (2000) *Phys. Rev. E Stat. Phys. Plasmas Fluids Relat. Interdiscip. Top.* **62,** 4000–4009
21. Seddon, J. M. (1990) *Biochim. Biophys. Acta* **1031,** 1–69
22. Ellens, H., Bentz, J., and Szoka, F. C. (1985) *Biochemistry* **24,** 3099–3106
23. Bartlett, G. R. (1959) *J. Biol. Chem.* **234,** 469–471
24. Griffith, O. H., Lesch, G. H., Rempfer, G. F., Birrell, G. B., Burke, C. A., Schlosser, D. W., Mallon, M. H., Lee, G. B., Stafford, R. G., Jost, P. C., and Marriott, T. B. (1972) *Proc. Natl. Acad. Sci. U.S.A.* **69,** 561–565
25. Galanos, C., Lüderitz, O., and Westphal, O. (1969) *Eur. J. Biochem.* **9,** 245–249
26. Brandenburg, K., Jürgens, G., Andrä, J., Lindner, B., Koch, M. H., Blume, A., and Garidel, P. (2002) *Eur. J. Biochem.* **269,** 5972–5981
27. Jürgens, G., Müller, M., Garidel, P., Koch, M. H., Nakakubo, H., Blume, A., and Brandenburg, K. (2002) *J. Endotoxin. Res.* **8,** 115–126
28. Japelj, B., Pristovsek, P., Majerle, A., and Jerala, R. (2005) *J. Biol. Chem.* **280,** 16955–16961
29. Zorko, M., Japelj, B., Hafner-Bratkovic, I., and Jerala, R. (2009) *Biochim. Biophys. Acta* **1788,** 314–323
30. Japelj, B., Zorko, M., Majerle, A., Pristovsek, P., Sanchez-Gomez, S., Martinez de Tejada, G., Moriyon, I., Blondelle, S. E., Brandenburg, K., Andrä, J., Lohner, K., and Jerala, R. (2007) *J. Am. Chem. Soc.* **129,** 1022–1023
31. Wimley, W. C., Creamer, T. P., and White, S. H. (1996) *Biochemistry* **35,** 5109–5124
32. Yang, N., Strøm, M. B., Mekonnen, S. M., Svendsen, J. S., and Rekdal, O. (2004) *J. Pept. Sci.* **10,** 37–46
33. Blondelle, S. E., and Lohner, K. (2000) *Biopolymers* **55,** 74–87
34. Wilkinson S. G. (1988) in *Microbial Lipids* (Ratledge C., and Wilkinson S. G., eds) pp. 299–488, Academic Press, London
35. White, D. A., Lennarz, W. J., and Schnaitman, C. A. (1972) *J. Bacteriol.* **109,** 686–690
36. Eklund, K. K., Salonen, I. S., and Kinnunen, P. K. (1989) *Chem. Phys. Lipids* **50,** 71–78
37. Latal, A., Degovics, G., Epand, R. F., Epand, R. M., and Lohner, K. (1997) *Eur. J. Biochem.* **248,** 938–946
38. Rappolt, M., Hickel, A., Bringezu, F., and Lohner, K. (2003) *Biophys. J.* **84,** 3111–3122
39. Sun, H., Greathouse, D. V., Andersen, O. S., and Koeppe, R. E., 2nd (2008) *J. Biol. Chem.* **283,** 22233–22243
40. Willumeit, R., Kumpugdee, M., Funari, S. S., Lohner, K., Navas, B. P., Brandenburg, K., Linser, S., and Andrä, J. (2005) *Biochim. Biophys. Acta* **1669,** 125–134
41. Andrä, J., Lohner, K., Blondelle, S. E., Jerala, R., Moriyon, I., Koch, M. H., Garidel, P., and Brandenburg, K. (2005) *Biochem. J.* **385,** 135–143
42. Brandenburg, K., Howe, J., Sánchez-Gómez, S., Garidel, P., Roessle, M., Andrä, J., Jerala, R., Zweytick, D., Lohner, K., Rappold, M., Blondelle, S. E., Moriyon, I., and Martinez-de-Tejada, G. (2010) *Anti-Infective Agents Med. Chem.* **9,** 9–22
43. Lockwood, N. A., Haseman, J. R., Tirrell, M. V., and Mayo, K. H. (2004) *Biochem. J.* **378,** 93–103
44. Deutsch, G. (2006) *Modulation of Membrane Perturbation by N-Acylated Peptides Derived from a Human Lactoferrin Fragment.* Ph.D. thesis, Graz University of Technology, Graz, Austria